Investigation of nitride layers deposited on annealed AISI H13 steel by die-sinking electrical discharge machining

Sinval Pedroso da Silva[1] · Alexandre Mendes Abrão[2] · Peter Georg Weidler[3] · Ernane Rodrigues da Silva[4] · Marcelo Araújo Câmara[2]

Abstract

The performance of electrical discharge machining is dependent mainly on the dielectric fluid and process parameters. Significant attention has been drawn to introducing alternative dielectric fluids in order to achieve superior surface integrity and higher productivity. However, there is a challenge in producing more uniform surface layers in the emerging nitriding process by electrical discharges. Thus, this work studies the relationship between process parameters and the features of the layers produced using surface modification by die-sinking electrical discharge machining employing urea $[(NH_2)_2CO]$ in deionized water as dielectric fluid. The influence of pulse-on time and pulse-off time on the uniformity and thickness of the recast layer, heat-affected zone, and depth of hardened layer was investigated. The experimental work employed annealed AISI H13 tool steel as base material and electrolytic copper as electrode. In order to characterize the samples and investigate the modifications produced by the process, chemical analysis, optical microscopy, scanning electron microscopy, X-ray diffraction, and microhardness measurements were used. The results indicated an evident influence of the process parameters on uniformity and thickness of the layers. The thickest altered metal zone layer obtained was 53.2 ± 5.5 μm when both pulse-on and -off times of 500 μs were used, while the smallest thickness of 31.0 ± 4.6 μm was obtained for both pulse times of 100 μs. The investigated process increased the surface hardness about three times compared with the non-processed AISI H13 steel. This can be attributed to the iron nitrides such as $Fe_{11}N$ found in the samples.

Keywords AISI H13 tool steel · EDM · Microhardness · Nitriding · Surface modification · XRD

Nomenclature

α	Significance level
AMZ	Altered metal zone
ANOVA	Analysis of variance
COD	Crystallography open database
CI	Confidence interval
D_T	Duty factor [%]
EDS	Energy-dispersive spectroscopy
HAZ	Heat-affected zone
ICSD	Inorganic Crystal Structure Database
I_p	Peak current [A]
OES	Optical emission spectrometry
RL	Recast layer
p value	Probability value

✉ Sinval Pedroso da Silva
sinvalpedroso@yahoo.com.br

Alexandre Mendes Abrão
abrao@demec.ufmg.br

Peter Georg Weidler
peter.weidler@kit.edu

Ernane Rodrigues da Silva
ernane@cefetmg.br

Marcelo Araújo Câmara
marcelocamara@demec.ufmg.br

[1] Postgraduate Program in Mechanical Engineering (PPGMEC), Universidade Federal de Minas Gerais, Av. Presidente Antônio Carlos, 6627, Pampulha, Belo Horizonte, MG 31270 901, Brazil

[2] Mechanical Engineering Department, Universidade Federal de Minas Gerais, Av. Presidente Antônio Carlos, 6627, Pampulha, Belo Horizonte, MG 31270 901, Brazil

[3] Institute of Functional Interfaces, Karlsruhe Institute of Technology, P.O. Box 3640, 76021 Karlsruhe, Germany

[4] Postgraduate Program in Materials Engineering (POSMAT), Centro Federal de Educação Tecnológica de Minas Gerais, Av. Amazonas, 5253, Nova Suiça, Belo Horizonte, Minas Gerais 30480 000, Brazil

SM-SEDM	Surface modification by die-sinking electrical discharge machining
SEM	Scanning electron microscopy
t_{AMZ}	Thickness of altered metal zone
t_{HAZ}	Thickness of heat-affected zone
T_{OFF}	Pulse-off time [μs]
T_{ON}	Pulse-on time [μs]
t_{RL}	Thickness of recast layer
U	Discharge voltage [V]
XRD	X-ray diffraction

1 Introduction

Electrical discharge machining (EDM) is applied for electrically conductive materials with the thermoelectric working principle in which the thermal energy of a spark is used to remove material from the workpiece [1]. The EDM input parameters [e.g., peak current (I_p), pulse-on time (T_{ON}), pulse-off time (T_{OFF}), discharge voltage (U), working time, nozzle flushing] affect the process aiming at improving its performance, e.g., material removal rate, surface finishing, tool wear rate [2], and corrosion resistance [3, 4]. Nevertheless, a rather limited number of EDM machining parameters and few settings have been tried by researchers and most of them show the remarkable influence of I_p and T_{ON} on the EDM performance [5]. Therefore, there is a need to independently study the effect of T_{OFF} as this is an important input process parameter on the phenomenon of surface modification [6].

The EDM process changes not only the surface of the workpiece metal, but alters also the metallurgical structure and characteristics of subsurface [7] once the discharge temperature reaches up to 12,000 °C [8]. On the top of the unaffected base metal, a molten and resolidified layer is observed, named as recast layer (RL). This layer is formed by the unexpelled molten metal solidifying in the crater [6] from the dielectric fluid cooled at very high cooling rate. Adjacent to the RL is the heat-affected zone (HAZ) or annealed layer, which was not melted but influenced by high temperatures [7]. The depth of the RL and the HAZ is determined by the heat sinking ability of the material and the power applied (pulse energy and duration). With this regard, the discharge energy—determined by the I_p and T_{ON} [9], assuming a constant discharge voltage [10]—is the main responsible for the depth of hardened layer.

Klocke et al. [9] studied the relationship between discharge energy and the thickness of recast layer (t_{RL}) and stated that a higher discharge energy results in a thicker RL. This is caused by a larger amount of metal which melts and resolidifies on the surface, as also observed by Guu et al. [11] and Rebelo et al. [12]. Similarly, the thickness of the heat-affected zone (t_{HAZ}) is influenced by discharge energy, i.e., the higher

average discharge energy, the thicker HAZ [9]. This means that the more energy dissipates into the workpiece, the deeper the temperature reaches the recrystallization level and recrystallization takes place [9].

The field of surface modification using EDM is at the experimental stage. Some topics of interest are (i) workpiece surface modification using chemical elements present in the dielectric fluid [6, 13–15], transfer of chemical elements from powder metallurgy (PM) electrodes (e.g., WC-Co) to the workpiece surface (e.g., AISI H13) [16, 17], and alloyed workpiece surface layer (e.g., the formation of a TiC layer in a high speed steel substrate) [18]. In some cases, powders are added and mixed in the dielectric fluid (e.g., Al, Cr, graphite, SiC, Ti, etc.), named after powder mixed EDM. The feasibility of the surface modification process is established, although many issues need to be addressed before the method can be formally accepted by industry [6]. For instance, one of the issues to be addressed is the non-uniformity of the layers formed in the case of surface modification by die-sinking electrical discharge machining (SM-SEDM) using deionized water as dielectric, as indicated by [19, 20]. For Marashi et al. [4], among various types of dielectric used in powder mixed EDM, hydrocarbon oil, such as mineral oil or kerosene, is still the most common and efficient die-sinking EDM dielectric fluid. Nevertheless, water has found increasing application in recent years due to (i) healthier and safer operational environment; (ii) deionized water can be a favorable choice in some EDM applications owing to its lower viscosity, higher thermal conductivity, and higher flow rate compared with hydrocarbon oil dielectrics. Most of the published research works on powder mixed EDM have studied its effects on material remove rate, surface finishing, and tool wear rate. However, very few works have taken up the study of the effects of powder mixed EDM method on surface modification [6], and only a few investigations have considered the addition of powder to water as dielectric fluid.

The hardness of the machined surface is also affected by SM-SEDM, by powder mixed EDM or by using PM electrodes. Yan, Tsai, and Huang [21] employed distilled water and distilled water with urea (10 g L^{-1}) as dielectric fluids during EDM of pure titanium. The authors obtained higher cross section microhardness values of the samples produced with urea solution in comparison with distilled water. In addition to that, the hardened layer obtained with urea solution was approximately 80 μm thick, while the hardened layer produced with distilled water was 50 μm thick. This effect was explained by the decomposition of nitrogen from the urea solution dielectric, with nitrogen enrichment evenly distributed on the machined surface that resulted in a TiN hard layer produced on the titanium surface, which exhibited improved friction and wear characteristics [21]. Santos et al. [22] found that surface hardening occurs in both cases: with deionized water only and with a solution of urea in deionized water as

dielectric fluids. However, the microhardness values on the RL and HAZ were higher for the samples machined with a solution of urea as dielectric fluid in comparison with deionized water. Furthermore, the hardness of the RL of the samples machined with a solution of urea was higher than that of the HAZ. It is suggested that the amount of nitrides is larger in the RL than in the HAZ, which is reasonable since the nitrogen concentration decreases with the distance from the surface. This phenomenon was suggested by [22], who detected highest concentration of nitrogen on the surface, which reduced gradually below the machined surface. The presence of urea in the dielectric fluid did not alter the typical morphology of the machined surfaces in comparison with deionized water [22]. Çoğun, Özerkan, and Karaçay [5] studied the variation of surface hardness with different T_{ON} (25 and 100 μs) and found that increasing T_{ON} increases the hardness of the machined surface. This is mainly due to thicker resolidified layer formed by the higher discharge energy. The hardness values for both powders (H_3BO_3 and graphite) used during machining were higher than for the pure kerosene used as base dielectric. Aspinwall et al. [17] obtained an increase in hardness of up to 100% of AISI H13 steel processed by die-sinking EDM, which can be attributed to factors as I_p, T_{ON}, and the presence of elements from PM electrode on the machined surface.

With regard to steel grades and their applications, high-alloy steels as AISI H13 hot work die steel provide a compromise between resistance to thermal softening (wear) and reasonable toughness. AISI H13 steel is especially suitable for press dies as well as for hammer applications in which the amount of parts to be forged is large and wear resistance becomes an important economic requirement [23]. Some of the chemical elements for AISI H13 (e.g., Cr, Mo, V) form hard carbides, which contribute to wear resistance. Nitriding on parts manufactured with AISI H13 steel offers additional wear resistance [24].

In this work, the surface modification by die-sinking electrical discharge machining (SM-SEDM) of AISI H13 steel using electrolytic copper as electrode and a solution of urea [$(NH_2)_2CO$] in deionized water as dielectric fluid (concentration of 30 g L^{-1}) is proposed. According to [25, 26], the solubility of urea (minimum purity of 99.98% certified ACS-grade) in double-distilled water is 121.0 g in 100 g of H_2O (1206.3 g L^{-1}) at 25.5 °C. The influence of T_{ON} and T_{OFF} on the formation of RL and HAZ was investigated, aimed at identifying the conditions related to the set of parameters, defined experimentally based on preliminary tests, responsible for better uniformity of the RL and HAZ, as well as thicker hardened layer after nitriding by SM-SEDM. Furthermore, nitride formation simultaneously to electrical discharge machining of AISI H13 steel was evaluated. Prior to the experimental work, the electrical discharge machine was adapted (development of a new system with an auxiliary tank to deliver the dielectric fluid) in order to enable the application of SM-SEDM.

2 Materials and methods

Annealed AISI H13 tool steel samples (25.40 mm diameter × 12.00 mm thickness) with an average hardness of 214 ± 2 HV$_{0.5}$ were used as base material and C11000 UNS class electrolytic copper (31.75 mm diameter × 40.00 mm length) was employed as electrode.

An Engemaq EDM 200 NC L series die-sinking electrical discharge machine (maximum electric current of 60 A) was adapted to perform SM-SEDM, as follows: in order to avoid contamination of the usual EDM dielectric fluid, a tank (capacity for 62 L) was designed and built to work with aqueous fluids. It is placed inside the original machine tank, as shown in Fig. 1. An open flushing system composed of a motor-pump (power of 120 W, flow rate of 62 L min^{-1}, and pressure of 0.7 bar) and dielectric fluid orienting pipe was used to supply the dielectric fluid during SM-SEDM treatment.

The process parameters used in this work are shown in Table 1. Six sets of operational parameters (I to VI), defined experimentally based on preliminary tests, were selected and the main goal was to investigate the influence of different T_{ON} and T_{OFF} on the formation of RL and HAZ. For all tests, the white crystalline granular urea (nitrogen source) dissolved in deionized water was used as a dielectric fluid at a concentration of 30 g L^{-1}, defined based on preliminary tests that resulted in good agreement with hardness, electrical conductivity of the solution, and consumption of urea. Urea contains 46.6% of nitrogen in its composition, with 25.5% nitrogen in the saturated solution (1206.3 g L^{-1} at a temperature of 25.5 °C). However, according to [20, 21], the increase in the amount of urea (higher than 10 g L^{-1}) in pure water can influence the electrical conductivity, which affects the performance of the process (e.g., formation of the plasma channel and material removal rate). Therefore, using deionized water (0 μS cm^{-1}) as a solvent, it was observed in this work that, when adding 30 g L^{-1} of high purity urea (99.5%), the average electrical conductivity remained low (13 ± 1 μS cm^{-1} at the beginning of the test and 21 ± 1 μS cm^{-1} at the end of the experiments with SM-SEDM). Based on that, and the fact that variations in the urea content did not significantly change the thickness of the nitride layer and the hardness of the surface, the concentration of 30 g L^{-1} was defined for this work. Furthermore, if the urea concentration increases (e.g., doubling from 30 to 60 g L^{-1}), there will be a difference of only approximately 0.65% of nitrogen in the solution, which does not contribute significantly to higher nitrogen migration to the surface and subsurface of the samples. For the tests, the conductivity of the dielectric fluid was monitored using a portable

Fig. 1 Schematics of SM SEDM system used in the experimental work
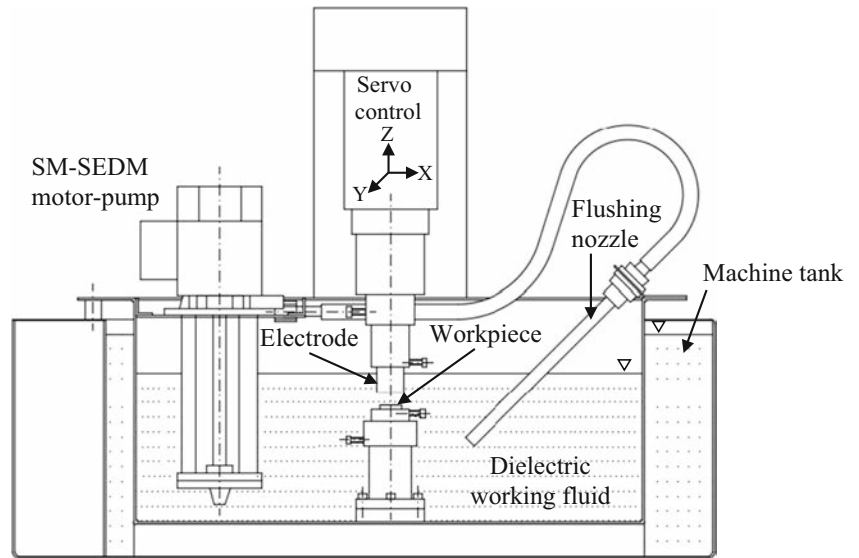
conductivity meter (range 0–1999 μS cm^{-1}, temperature 1–80 °C, and accuracy of ± 1 digit).

The duration of each test was 15 min for roughing (51.45 A) and 20 min for finishing (6.86 A), determined in preliminary tests and aiming at ensuring spark erosion of the entire workpiece surface. Each test was performed three times and the average values are report.

Chemical analysis of AISI H13 steel and electrolytic copper electrode samples was carried out by optical emission spectrometry (OES) in a SPECTRO SPECTROMAXx LMX equipment. Vickers microhardness tests were conducted on cross sections of AISI H13 steel samples using a Shimadzu HMV-2TE automatic microtester with a load of 25 gf and 20 s dwell time. The phase compositions on AISI

Table 1 Experimental work parameters used for SM SEDM

Fixed parameters			Description			
Dielectric fluid			Urea in deionized water			
Dielectric concentration			30 [g L^{-1}]			
Tool electrode			Electrolytic copper			
Tool electrode polarity			Positive [+]			
Erosion time			0.8 [s]			
Periodic electrode retraction			2 [mm]			
Distance between the electrode and workpiece (gap)			1 5			
Sensitivity of servomechanism			1 5			
Roughing operation						
Peak current, I_p			51.45 [A]			
Test duration			15 [min]			
Set of parameters	**I**	**II**	**III**	**IV**	**V**	**VI**
Pulse on time, T_{ON} [μs]	100	100	100	100	500	500
Pulse off time, T_{OFF} [μs]	43	100	150	203	500	1015
Duty cycle, D_T [%][a]	70	50	40	33	50	33
Finishing operation						
Peak current, I_p			6.86 [A]			
Test duration			20 [min]			
Set of parameters	**I**	**II**	**III**	**IV**	**V**	**VI**
Pulse on time, T_{ON} [μs]	10	10	10	10	50	50
Pulse off time, T_{OFF} [μs]	4	10	15	20	50	102
Duty cycle, D_T [%]	70	50	40	33	50	33

[a] Duty cycle [(T_{ON} / (T_{ON} + T_{OFF})) × 100], D_T [%]

H13 steel samples before and after the SM-SEDM were obtained with a Shimadzu XRD-7000 diffractometer using Cu Kα1 radiation ($\lambda = 1.540562$ Å). Data were collected at a tube voltage of 40 kV and a current of 30 mA at a step size of 0.02° 2θ for a scan step time of 5 s over an angular range of 30° to 110° 2θ. The obtained diffractograms were analyzed with the DIFFRAC.EVA 5.2 software by Bruker AXS, Germany [27]. The XRD patterns were interpreted by comparison with the cards of the Crystallography Open Database (COD) [28] and the Powder Diffraction Files (PDF) from the Inorganic Crystal Structure Database (ICSD).

3 Results and discussion

3.1 Material characterization

Tables 2 and 3 show, respectively, the chemical compositions of AISI H13 steel and electrolytic copper samples used in the SM-SEDM experiments. The presence of chemical elements such as Cr, Mo, and V, which favor nitriding, can be noticed in AISI H13 steel (Table 2) and the corresponding amounts are in accordance with ASTM standard [29].

Table 3 shows that the composition of electrolytic copper electrodes is in accordance with the literature [30]: 99.90% Cu (min) and 0.04% O for UNS C11000 class electrolytic copper.

Figure 2 presents results concerned with AISI H13 steel cross section. Figure 2 a shows a scanning electron microscopy (SEM) image of the microstructure etched in 2% Nital and obtained by secondary electrons. Figure 2 b shows the semi-quantitative chemical composition analysis (wt.%) by energy-dispersive spectroscopy (EDS), performed in six different regions of the SEM image and Fig. 2c shows the X-ray diffractogram. It can be noted in Fig. 2a that the microstructure of AISI H13 steel consists of spheroidized carbides uniformly dispersed in a ferrite matrix. This microstructure is typical of annealed AISI H13 steel. The semi-quantitative analysis by EDS, see Fig. 2b, indicates the presence of Cr, V, Si, and Fe, and Fig. 2c indicates the presence of ferrite (α-Fe), (Cr, Fe)$_7$C$_3$, and Cr$_3$C$_2$ carbides. These results corroborate with Roberts, Krauss, and Kennedy [31], who state that the equilibrium structure at room temperature of the annealed AISI H13 steel is M$_7$C$_3$ carbides in a ferrite matrix (M denotes a

Table 2 AISI H13 steel chemical composition (wt.%)

Element	Concentration	Element	Concentration
Fe	91.145	Mn	0.367
Cr	4.738	V	0.802
Mo	1.226	Cu	0.058
C	0.380	Others	0.350
Si	0.935		

Table 3 Electrolytic copper chemical composition (wt.%)

Element	Concentration	Element	Concentration
Cu	99.902	Ni	0.006
Zn	0.022	C	0.005
Te	0.020	Al	0.004
Co	0.014	S	0.003
Bi	0.009	Others	0.015

transition metal, e.g., Cr and Fe). These data are in agreement with results from the Fe-Cr-C system alloys containing 5% chromium, as AISI H13 steel [31].

The average Vickers microhardness of AISI H13 as received steel is 214 ± 2 HV$_{0.5}$, with a 95% confidence interval (CI). This result agrees with data from the manufacturer which indicates a maximum hardness of 207 HB (approximately 218 HV [32]).

3.2 Influence of SM-SEDM parameters on the deposited nitride layer

Figure 3 shows the microhardness profile beneath the surface of AISI H13 steel after SM-SEDM. The higher hardness values (above 800 HV$_{0.025}$) are observed near the surface and are related to the RL. These values decrease rapidly, indicating the transition zone between the RL and HAZ. However, the decrease in hardness is steeper for the samples obtained using $T_{ON} = 100$ μs and resulted thinner hardened layers. In contrast, thicker hardened layers were obtained after SM-SEDM with $T_{ON} = 500$ μs. This behavior can be explained by to the higher discharge energy ($I_p \times T_{ON} \times U$) applied to the samples produced using $T_{ON} = 500$ μs, which promotes a deeper modification beneath the surface. In general, the hardness values stabilize at approximately 285 HV$_{0.025}$ at distance of 61.4 μm from the surface. Thus, the hardness limit (H limit) of 340 HV$_{0.025}$ was considered as the baseline to define the depth of the hardened layer after nitriding, according to DIN [33] and ISO [34] criteria (H limit = core actual hardness + 50 HV, rounded by 10 HV).

Based on the microhardness profiles of each set of parameters (I to VI) studied in this work, Table 4 shows the values of the depth of hardened layer after nitriding using SM-SEDM. The depth of hardened layer with $T_{ON} = 500$ μs is larger than with $T_{ON} = 100$ μs. This corroborates with the data by [9, 11, 12, 35], who observed that higher discharge energy ($I_p \times T_{ON} \times U$) results in thicker RL and thicker HAZ. T_{ON} is directly proportional to the thickness of the HAZ [9].

Table 5 shows the analysis of variance (ANOVA) for the depth of the hardened layer after nitriding with 95% confidence level ($\alpha = 0.05$). The factor represented by samples with different T_{ON} and T_{OFF} presented a probability value (p value) of 0.000, which leads to considering that the obtained results

Fig. 2 AISI H13 steel: **a** SEM microstructure image, **b** semi quantitative chemical composition (wt. and atomic %) by EDS, and **c** X ray diffractogram

Element	(Wt.%)	(Atom.%)
C	14.7 ±2.5	43.8 ±4.2
Cr	5.2 ±1.2	3.6 ±0.6
V	0.9 ±0.4	0.7 ±0.2
Si	0.9 ±0.3	1.1 ±0.3
S	0.9 ±1.2	0.9 ±1.1
Fe	77.4 ±5.3	50.0 ±6.2

(a)   (b)

(c)
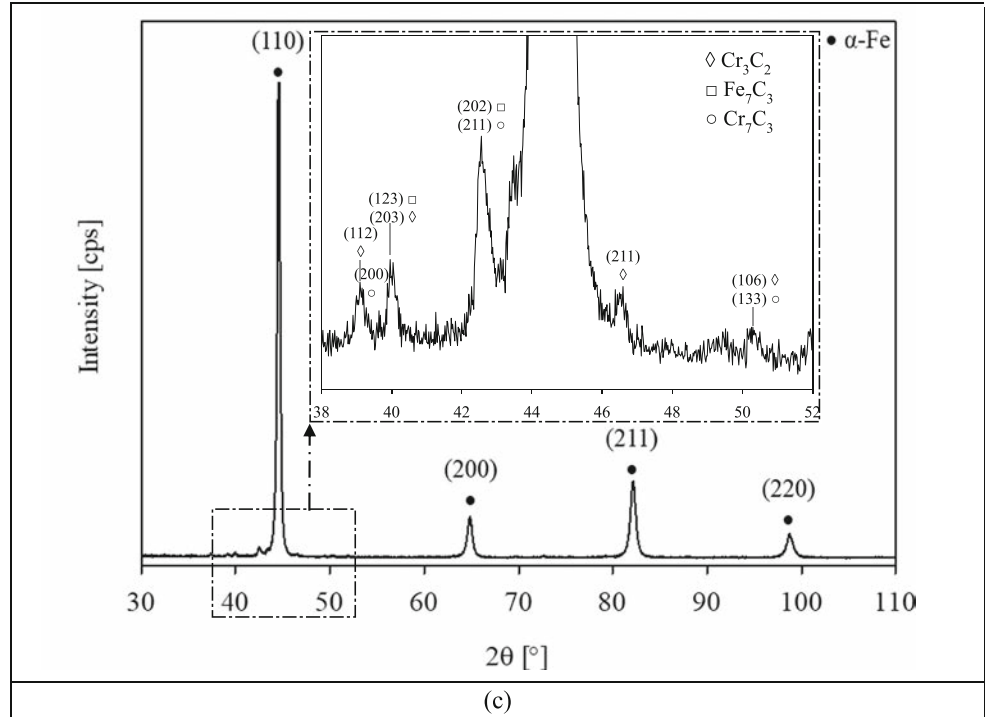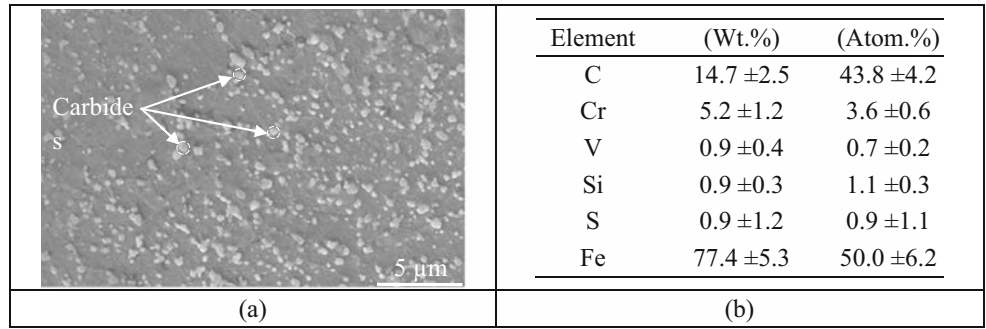
Fig. 3 Microhardness profile of AISI H13 after SM SEDM with different T_{ON} and T_{OFF}
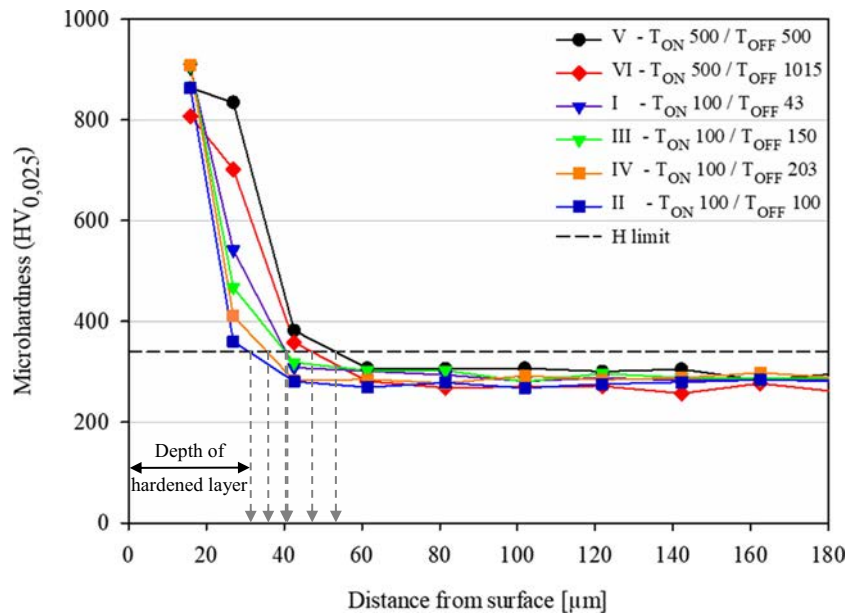
Table 4 Depth of the hardened layer after nitriding with different T_{ON} and T_{OFF}

Set of parameters	I	II	III	IV	V	VI
Roughing						
Pulse on time, T_{ON} [μs]	100	100	100	100	500	500
Pulse off time, T_{OFF} [μs]	43	100	150	203	500	1015
Finishing						
Pulse on time, T_{ON} [μs]	10	10	10	10	50	50
Pulse off time, T_{OFF} [μs]	4	10	15	20	50	102
Nitride depth [μm] at H limit of 340 $HV_{0.025}$	40.4 ± 3.8	31.0 ± 4.6	40.3 ± 1.7	35.6 ± 0.6	53.2 ± 5.5	47.2 ± 1.4

are statistically significant [36]. Therefore, the null hypothesis (H_0) can be rejected in favor of the alternative hypothesis (H_1), which indicates that there is a relation between T_{ON} and T_{OFF} with the depth of the hardened layer produced by nitriding via SM-SEDM.

Based on the Tukey test shown in Table 6, the selected sets of parameters (I to VI) resulted in significant differences in relation to the thickness of the hardened lay, represented by the response data "thickness of the hardened layer after nitriding". The sets of parameters V and VI employed a T_{ON} of 500 μs for roughing followed by 50 μs for finishing, which resulted in highest thickness mean values, while the remaining sets of parameters used a T_{ON} of 100 μs for roughing and 10 μs for finishing. This indicates that T_{ON} influences the thickness of the hardened layer after nitriding by SM-SEDM.

Figure 4 presents the boxplot of depth of the hardened layer after nitriding by SM-SEDM, based on the hardness limit (H limit) of 340 $HV_{0.025}$, versus the set of parameters (I to VI) with different pulse-on times and pulse-off times (T_{ON}/T_{OFF}). The samples with $T_{ON} = 100$ μs showed lower nitride layer depth, while the samples with T_{ON}/T_{OFF} of 500/500 μs showed higher average value (53.2 μm), followed by T_{ON}/T_{OFF} of 500/1015 μs (47.2 μm). This can be attributed to the higher discharge energy during nitriding of the samples with $T_{ON} = 500$ μs. Since during the processing of the samples with the highest T_{OFF} (1015 μs) in combination with the other parameters used on this work (according to Table 1), it was noticed that there was arcing effect and instability. These results corroborate the work by Chounde and Pawar [2], who

state that the higher I_p will result in increasing pulse discharge energy. Moreover, an inappropriate combination of T_{ON}, I_p, and duty cycle (D_T), which is related to T_{OFF}, may cause arcing effect or instability. Thus, despite the fact that the depth of the hardened layer after nitriding of the samples produced with T_{ON}/T_{OFF} of 500/500 μs against 500/1015 μs is statistically similar. The results obtained under the former condition are considered the most appropriate to produce the thickest hardened layer by SM-SEDM with urea solution, as it does not promote arcing effect.

Figure 5 shows the X-ray diffractograms (θ-2θ configuration) performed after SM-SEDM with different T_{ON} and T_{OFF} compared with the AISI H13 steel base material. Some peaks for SM-SEDM samples at 43.0°, 50.7°, 74.5°, and 90.2° 2θ, as well as change of peaks with 2θ of 44.6°, 64.7°, 82.1°, and 98.6°, were recorded. There is an appreciable similarity for all XRD spectra of SM-SEDM samples. The major phase of the surface layer after SM-SEDM is iron nitride ($Fe_{11}N$), originated from the $FeN_{0.0950}$ phase [37], space group Fm-3 m (225). The presence of iron nitride justifies the increase in hardness (shown in Fig. 3) on the surface and subsurface after the SM-SEDM treatment.

In order to perform further characterization of the layers produced by SM-SEDM, it was used optical microscopy analysis and Vickers microhardness measurements. Figure 6 presents images of AISI H13 sample cross section after SM-SEDM. The analysis of the images indicates a lighter layer on the surface and a second layer just below it. These layers were produced during the SM-SEDM and they represent the RL and the HAZ, respectively. The formation of a more

Table 5 Analysis of variance (ANOVA) for hardened layer thickness

Source of variation	Degrees of freedom	Sum of squares	Contribution ratio [%]	Mean square	F value	p value
Samples	5	1297.00	90.19	259.40	22.05	0.000
Error	12	141.10	9.81	11.76		
Total	17	1438.20	100.00			
R^2	90.19%					

H_0: $\beta_1 = 0$
H_1: $\beta_1 \neq 0$

Table 6 Tukey test for thickness of the hardened layer after nitriding

Set of parameters	T_{ON}/T_{OFF} parameter		Thickness of the hardened layer after nitriding [μm]*
	Roughing	Finishing	
V	500/500	50/50	$53.2^a \pm 5.5$
VI	500/1015	50/102	$47.2^a \pm 1.4$
III	100/150	10/15	$40.3^b \pm 1.7$
I	100/43	10/4	$40.4^b \pm 3.8$
IV	100/203	10/20	$35.6^b \pm 0.6$
II	100/100	10/10	$31.0^b \pm 4.6$

*Means that do not share a letter ([a, b]) are significantly different by the Tukey method and 95% confidence

irregular RL and HAZ thickness is observed in Fig. 6 a, b, c and d in comparison to Fig. 6 e and f. Irregularities of melted and resolidified material on the surface of samples in Fig. 6 a, b, c, d and f are observed. That indicates that the T_{ON} and T_{OFF} are not adequate to meet the proposed goal of obtaining better uniformity of these layers. The uniform and thickest layer is obtained using T_{ON} and T_{OFF} both of 500 μs, as shown in Fig. 6e. Moreover, it suggests that the combination of high T_{ON} with high T_{OFF} contributes to a higher electrical discharge energy while it provides favorable conditions for the working gap (e.g., off time for adequate flushing) and consequently contributed to less accumulation of particles and molten material, deposited irregularly on the workpiece surface. The test configuration with $T_{ON} = 500$ and $T_{OFF} = 1015$ μs shown in Fig. 6f presents thicker layer, though not uniform. This suggests that arcing effect and instability occur during the SM-SEDM of those samples. The distance between electrode and the workpiece became unstable for T_{OFF} values greater than T_{ON} combined with the I_p used, thus confirming the work by Chounde and Pawar [2]. When the electrical discharge becomes unstable, it is necessary to reduce I_p. Furthermore, as a reduction on D_T means an increasing on the T_{OFF}, resulting in lower operation efficiency, since the workpiece material

removal rate is reduced [2, 38]. Thus, tests with D_T lower than 33% were not performed in this work.

It can also be noticed in the images of Fig. 6 that at the top, the layer of the sample cross section has a "white" aspect, that layer is related to the RL, while below the RL, the HAZ is present and the aspect is darker than the AISI H13 steel base material. The new phase found after SM-SEDM, $Fe_{11}N$ shown in Fig. 5, was obtained from these regions. However, the limits where there is no further formation of the new phase are not well established and, therefore, the microhardness profile was used to determine the depth of hardened layer after nitriding by SM-SEDM.

Figure 7 shows the results of the microhardness measurements performed on each cross section of the samples after SM-SEDM with different T_{ON} and T_{OFF}. The microhardness of the AISI H13 steel samples core was 285.7 ± 2.4 $HV_{0.025}$, as represented by the dashed red line in Fig. 7. However, the hardness values of the RL and HAZ layers are significantly higher than those of the core of AISI H13. The microhardness of RL is nearly 298% higher than that of the AISI H13 core. HAZ has a microhardness of approximately 198% higher than the AISI H13 core. These results indicate that surface hardening may be due to enrichment by nitrides on AISI H13 steel. In all investigated situations, the microhardness of RL is higher than that of HAZ, which is higher than that of the AISI H13 steel base material. These results suggest that the nitrogen concentration is higher on the surface than on the subsurface of AISI H13 steel after SM-SEDM.

The thicknesses of the recast layer (t_{RL}) and the altered metal zone (t_{AMZ}) were evaluated by optical microscopy. Figure 8 shows the average results of 20 measurements for each test condition (I to VI), represented by different T_{ON} and T_{OFF} for roughing. It is observed, as previously discussed, that the samples with T_{ON}/T_{OFF} of 500/500 μs and 500/1015 μs provide the highest layer thickness. According to ASM HANDBOOK [23], the thicker the nitride layer, the higher the wear resistance because the resistance against abrasion increases, thus increasing the component's life. This behavior is essential for tool steel applications subjected to abrasion
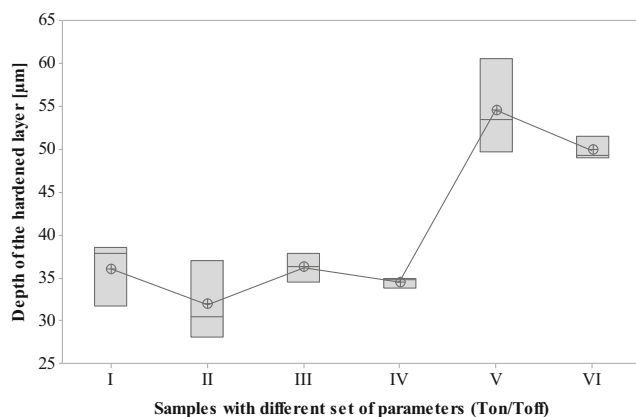
Fig. 4 Boxplot of depth of the hardened layer for samples with different T_{ON}/T_{OFF} (I 100/43; II 100/100; III 100/150; IV 100/203; V 500/500; and VI 500/1015)

Fig. 5 XRD patterns of AISI H13 base material and after SM SEDM with different T_{ON} and T_{OFF}
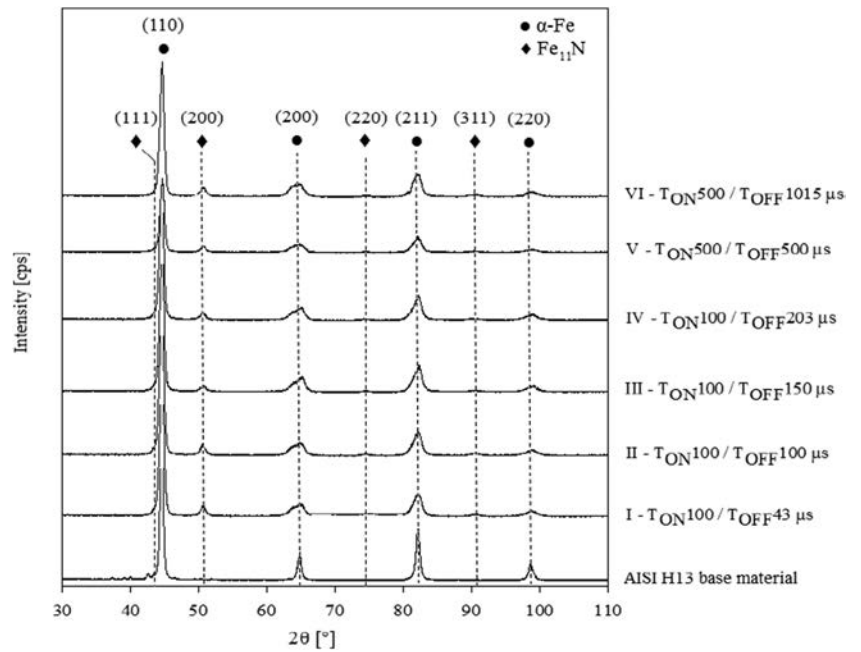
wear. In addition to that, similar behavior is expected against fatigue, since the increase in nitriding depth allows higher surface pressures and constant wear resistance, therefore recommending T_{ON}/T_{OFF} of 500/500 µs as the parameter responsible for the thickest AMZ (53.2 µm). The 500/500 µs T_{ON}/T_{OFF} working condition is more stable compared to T_{ON}/T_{OFF} of 500/1015 µs, as the latter showed arcing effect and instability.

4 Conclusions

This work has studied the effects of process parameters [(pulse-on time (T_{ON}) and pulse-off time (T_{OFF})] on surface modification by die-sinking EDM of annealed AISI H13 tool steel using a solution of urea in deionized water as dielectric fluid at 30 g L^{1} concentration. Six different sets of samples were produced and compared regarding depth of hardened layer and heat-affected zone (HAZ) uniformity and hardness, thicknesses of the recast layer (t_{RL}), and the altered metal zone (t_{AMZ}). Concluding remarks of the experimental work can be stated as follows:

- T_{ON} and T_{OFF} parameters influence the results of RL and AMZ thicknesses and uniformity of AISI H13 steel processed by SM-SEDM.
- The most favorable test configuration for thicker and uniform RL and HAZ studied in this work were T_{ON}/T_{OFF} of

(a) T_{ON} = 100 and T_{OFF} = 43 µs   (b) T_{ON} = 100 and T_{OFF} = 100 µs

(c) T_{ON} = 100 and T_{OFF} = 150 µs   (d) T_{ON} = 100 and T_{OFF} = 203 µs

(e) T_{ON} = 500 and T_{OFF} = 500 µs   (f) T_{ON} = 500 and T_{OFF} = 1015 µs
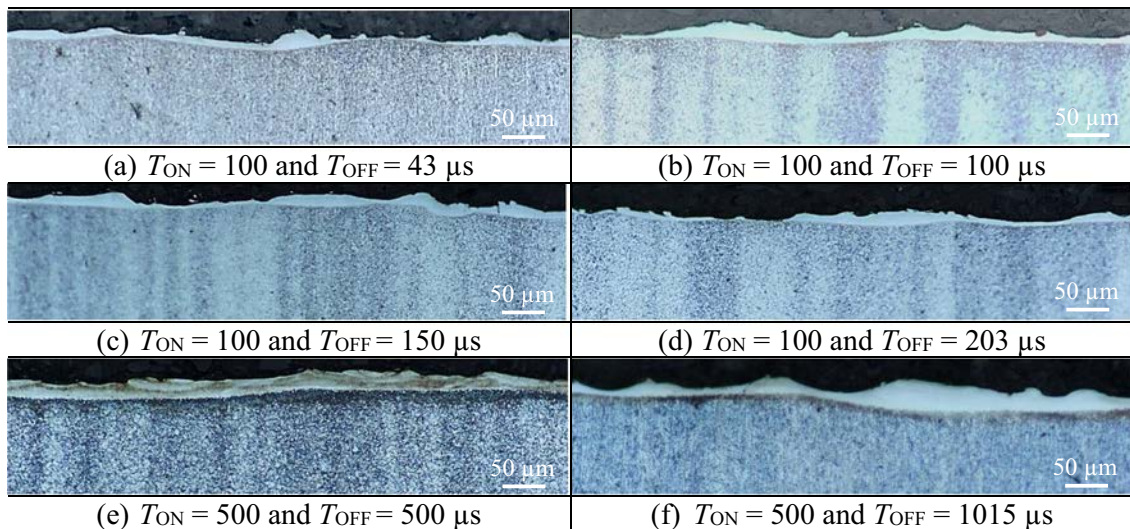
Fig. 6 AISI H13 steel cross section after SM SEDM treatment with different T_{ON} and T_{OFF}

Fig. 7 Effect of T_{ON} and T_{OFF} on microhardness
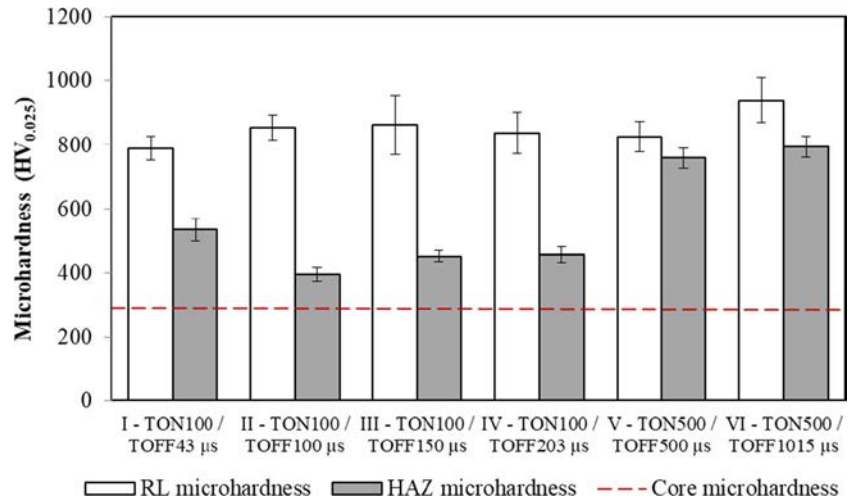
500/500 μs and 500/1015 μs. The T_{ON}/T_{OFF} of 500/500 μs sample configuration presented the thickest hardened layer (53.2 μm at the hardness limit of 340 $HV_{0.025}$), followed by T_{ON}/T_{OFF} of 500/1015 μs (47.2 μm). This can be attributed to the higher discharge energy with $T_{ON} = 500$ μs.

- SM-SEDM increased the surface hardness approximately three times compared with the non-processed AISI H13 steel, which can be attributed to the presence of iron nitrides, such as $Fe_{11}N$, found in the samples.
- The presence of nitrides on the AISI H13 steel samples after SM-SEDM is evident. The main nitride identified in this study is the $Fe_{11}N$ type, inferring dissociation of urea that introduces atomic nitrogen into the steel surface and subsurface.

Compliance with ethical standards

Conflict of interest The authors declare that they have no conflict of interest.

Fig. 8 Effect of T_{ON} and T_{OFF} on RL and AMZ thickness
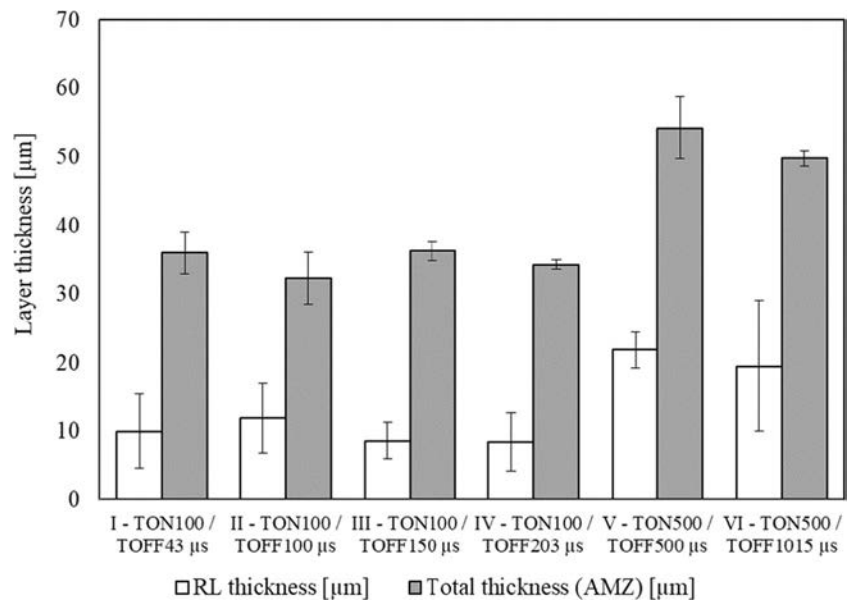
References

1. Jain VK (2009) Advanced machining processes. Allied publications pvt. limited, New Delhi
2. Chounde AB, Pawar M (2014) Study of pulsed DC power supply parameters for micro EDM. Int J Adv Res Electr Electron Instrum Eng 3:12493 12495. https://doi.org/10.15662/ijareeie.2014.0310033
3. Kansal HK, Singh S, Kumar P (2005) Parametric optimization of powder mixed electrical discharge machining by response surface methodology. J Mater Process Technol 169:427 436. https://doi.org/10.1016/j.jmatprotec.2005.03.028
4. Marashi H, Jafarlou DM, Sarhan AAD, Hamdi M (2016) State of the art in powder mixed dielectric for EDM applications. Precis Eng 46:11 33. https://doi.org/10.1016/j.precisioneng.2016.05.010
5. Çoğun C, Özerkan B, Karaçay T (2006) An experimental investigation on the effect of powder mixed dielectric on machining performance in electric discharge machining. Proc Inst Mech Eng B J Eng Manuf 220:1035 1050. https://doi.org/10.1243/09544054JEM320
6. Kumar S, Singh R, Singh TP, Sethi BL (2009) Surface modification by electrical discharge machining: a review. J Mater Process Technol 209:3675 3687. https://doi.org/10.1016/j.jmatprotec.2008.09.032
7. Kruth IP, Stevens I, Froyen I, Lauwers I (1995) Study of the white layer of a surface machined by die sinking electro discharge machining. CIRP Ann Manuf Technol 44:169 172. https://doi.org/10.1016/S0007 8506(07)62299 9
8. McGeough JA (1988) Advanced methods of machining. Chapman and Hall, New York
9. Klocke F, Schneider S, Ehle L, Meyer H, Hensgen L, Klink A (2016) Investigations on surface integrity of heat treated 42CrMo4 (AISI 4140) processed by sinking EDM. Procedia CIRP 42:580 585. https://doi.org/10.1016/j.procir.2016.02.263
10. Schumacher BM (2004) After 60 years of EDM the discharge process remains still disputed. J Mater Process Technol 149:376 381. https://doi.org/10.1016/j.matprotec.2003.11.060
11. Guu YH, Hocheng H, Chou CY, Deng CS (2003) Effect of electrical discharge machining on surface characteristics and machining damage of AISI D2 tool steel. Mater Sci Eng A 358:37 43. https://doi.org/10.1016/S0921 5093(03)00272 7
12. Rebelo JC, Dias AM, Kremer D, Lebrun JL (1998) Influence of EDM pulse energy on the surface integrity of martensitic steels. J Mater Process Technol 84:90 96. https://doi.org/10.1016/S0924 0136(98)00082 X
13. Chen HJ, Wu KL, Yan BH (2014) Characteristics of Al alloy surface after EDC with sintered Ti electrode and TiN powder additive. Int J Adv Manuf Technol 72:319 332. https://doi.org/10.1007/s00170 014 5669 y
14. Kumar S, Batra U (2012) Surface modification of die steel materials by EDM method using tungsten powder mixed dielectric. J Manuf Process 14:35 40. https://doi.org/10.1016/j.jmapro.2011.09.002
15. Li X, Wang D, Fang Y (2012) Study on die surface coating by electric discharging machining. Adv Mater Res 490 495:2619 2623. https://doi.org/10.4028/www.scientific.net/amr.490 495.2619
16. Simao J, Lee HG, Aspinwall DK, Dewes RC, Aspinwall EM (2003) Workpiece surface modification using electrical discharge machining. Int J Mach Tools Manuf 43:121 128. https://doi.org/10.1016/S0890 6955(02)00187 6
17. Aspinwall DK, Dewes RC, Lee HG, Simao J (2003) Electrical discharge surface alloying of Ti and Fe workpiece materials using refractory powder compact electrodes and Cu wire. CIRP Ann Manuf Technol 52:151 156. https://doi.org/10.1016/S0007 8506(07)60553 8
18. Suzuki T, Kobayashi S (2013) Mechanisms of TiC layer formation on high speed steel by a single pulse in electrical discharge machining. Electrochim Acta 114:844 850. https://doi.org/10.1016/j.electacta.2013.10.041
19. dos Santos RF, da Silva ER, Sales WF, Raslan AA (2017) Influence of the electrode material on the nitriding of medium carbon steel using sink electrical discharge machining. Int J Adv Manuf Technol 90:2001 2007. https://doi.org/10.1007/s00170 016 9531 2
20. dos Santos RF, da Silva ER, Sales WF, Raslan AA (2017) Influence of urea content blended with deionized water in the process of nitriding using electrical discharge machining on AISI 4140 steel. Int J Adv Manuf Technol 89:1251 1257. https://doi.org/10.1007/s00170 016 9159 2
21. Yan BH, Tsai HC, Huang FY (2005) The effect in EDM of a dielectric of a urea solution in water on modifying the surface of titanium. Int J Mach Tools Manuf 45:194 200. https://doi.org/10.1016/j.ijmachtools 2004.07.006
22. Santos RF, Silva ER, Sales WF, Raslan AA (2016) Analysis of the surface integrity when nitriding AISI 4140 steel by the sink electrical discharge machining (EDM) process. Procedia CIRP 45:303 306. https://doi.org/10.1016/j.procir 2016.01.197
23. ASM Handbook (1992) AMERICAN SOCIETY FOR METALS. Vol. 18. Friction, lubrication, and wear technology. ASM International®, Materials Park
24. ASM Handbook (2001) AMERICAN SOCIETY FOR METALS. Vol. 4. Heat treating. ASM International®, Materials Park
25. Lee FM, Lahti LE (1972) Solubility of urea in water alcohol mixtures. J Chem Eng Data 17:304 306. https://doi.org/10.1021/je60054a020
26. Pinck LA, Kelly MA (1925) The solubility of urea in water. J Am Chem Soc 47:2170 2172. https://doi.org/10.1021/ja01685a502
27. Bruker (2017) TOPAS V6: general profile and structure analysis software for powder diffraction data user's manual. Bruker AXS, Karlsruhe
28. Graulis S, Chateigner D, Downs RT et al (2009) Crystallography open database an open access collection of crystal structures. J Appl Crystallogr 42:726 729. https://doi.org/10.1107/S0021889809016690
29. ASTM International (2015) AMERICAN SOCIETY FOR TESTING AND MATERIALS. ASTM A681 08: standard specification for tool steels alloy. 08:1 14
30. ASM Handbook (1992) AMERICAN SOCIETY FOR METALS. Vol. 2. Properties and selection: nonferrous alloys and special purpose materials. ASM International®, Materials Park
31. Roberts G, Krauss G, Kennedy R (1998) Tool steels, 5th ed. ASM international®, materials park
32. ASTM International (2012) AMERICAN SOCIETY FOR TESTING AND MATERIALS. ASTM E140 Standard hardness conversion tables for metals relationship among Brinell hardness, Vickers hardness, Rockwell hardness, superficial hardness, Knoop hardness, scleroscope hardness, and Leeb hardness
33. DIN (1979) DIN 50190 3. Hardness depth of heat treated parts; determination of the effective depth of hardening after nitriding
34. ISO (2016) INTERNATIONAL ORGANIZATION FOR STANDARDIZATION. ISO 18203 Steel determination of the thickness of surface hardened layers (case depth)
35. Stambekova K, Lin HM, Uan JY (2012) Microstructural and corrosion characteristics of alloying modified layer on 5083 al alloy by electrical discharge alloying process with pure silicon electrode. Mater Trans 53:1436 1442. https://doi.org/10.2320/matertrans.M2012131

36. Montgomery DC (2013) Design and analysis of experiments, 8th edn. John Wiley & Sons, Inc., Hoboken

37. Jack KH (1951) The occurrence and the crystal structure of α'' iron nitride; a new type of interstitial alloy formed during the tempering of nitrogen martensite. Proc R Soc Lond Ser A Math Phys Sci 208: 216 224. https://doi.org/10.1098/rspa.1951.0155

38. Guitrau EB (1997) The EDM (electrical discharge machining) handbook. Hanser Gardner Publications, Cincinnati